

**Finite Element Analysis of Saint-Venant
Torsion Problem with Exact Integration of
the Elastic-Plastic Constitutive Equations**

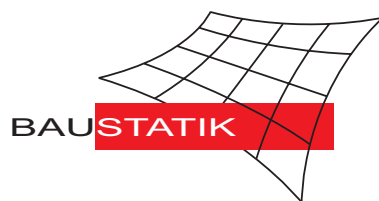
W. Wagner, F. Gruttmann

Mitteilung 3(1999)

Finite Element Analysis of Saint-Venant Torsion Problem with Exact Integration of the Elastic-Plastic Constitutive Equations

W. Wagner, F. Gruttmann

Mitteilung 3(1999)



© Prof. Dr.-Ing. W. Wagner Telefon: (0721) 608-2280
Institut für Baustatik Telefax: (0721) 608-6015
Universität Karlsruhe E-mail: bs@uni-karlsruhe.de
Postfach 6980 Internet: <http://www.bs.uni-karlsruhe.de>
76128 Karlsruhe

Finite Element Analysis of Saint-Venant Torsion Problem with Exact Integration of the Elastic-Plastic Constitutive Equations

W. Wagner
Institut für Baustatik
Universität Karlsruhe (TH)
Kaiserstraße 12
76131 Karlsruhe
Germany

F. Gruttmann
Institut für Statik
Technische Universität Darmstadt
Alexanderstraße 7
64283 Darmstadt
Germany

Abstract In this paper torsion of prismatic bars considering elastic–plastic material behaviour is studied. Based on the presented variational formulation associated isoparametric finite elements are developed. The unknown warping function is approximated using an isoparametric concept. The elastic–plastic stresses are obtained by an exact integration of the rate equations. Thus the ultimate torque can be calculated in one single load step. This quantity describes the plastic reserve of a bar subjected to torsion. Furthermore, for linear isotropic hardening no local iterations are necessary to compute the stresses at the integration points. The numerical results are in very good agreement with available analytical solutions for simple geometric shapes. The arbitrary shaped domains may be simply or multiple connected.

Keywords:

Pure torsion of prismatic bars, arbitrary cross–sections, exact integration of the elastic–plastic rate equations, isoparametric finite element formulation, ultimate torque

1 Introduction

The Saint–Venant torsion problem has been formulated as basic example for elasticity in many textbooks, e.g. [1, 2]. Introducing the so–called warping function the boundary value problem is described by a Laplacean equation and Neumann boundary conditions. The associated variational formulation is especially appropriated for a numerical solution using the finite element method. The essential advantage is given for multiple connected domains. Hence continuity conditions around the holes are automatically fulfilled. This is not the case when discretizing the stress function.

An experimental method to find the fully plastic solution is given with the so–called sand–heap analogy, Nadai [3]. Hereby sand is piled onto a horizontal table having the shape of the cross–section. The slope of the resulting heap cannot exceed the angle of internal friction which corresponds to the shear yield stress. Furthermore the membrane–roof analogy was introduced by Nadai for an experimental solution of the elastic–plastic torsion problem. Finite element solutions considering inelastic material behaviour have

been obtained e.g. by Yamada et al. [4]. Based on a hybrid stress method the authors developed triangular finite elements. Baba und Kajita [5] incorporated the normal stresses within the yield condition and developed rectangular finite elements. The authors in [4] and [5] applied explicit methods for an approximate integration of the rate equations. Hereby, critical time steps have to be considered.

The goal of this paper is to present efficient finite element formulations for the numerical analysis of the elastic–plastic torsion problem. In contrast to Ref. [4] and [5] the rate equations are integrated in an exact way. Thus, using line search techniques which guarantee global convergence the ultimate torque can be computed in one single load step. Furthermore, for linear isotropic hardening no local iterations are necessary to compute the stresses at the integration points. The numerical results are in very good agreement with available analytical solutions. Furthermore, the restrictions of rectangular elements [5] and the relative stiff behaviour of triangular elements [4] is overcome with the present isoparametric approach. The developed finite element formulation yields the ultimate torsion moment for arbitrary simply or multiple connected cross–sections. This section quantity is necessary to formulate yield conditions for spatial beams in terms of stress resultants, e.g. [2].

2 Saint–Venant torsion of a prismatic bar

We consider a prismatic bar whose longitudinal axis is the x –axis and whose cross–sections lie in the y – z –plane, see Fig. 1. The considered domain Ω with boundary $\partial\Omega$ may be multiple connected. On $\partial\Omega$ we define the right handed orthogonal basis system with tangent vector \mathbf{t} and outward normal vector $\mathbf{n} = [n_y, n_z]^T$. With \mathbf{t} the orientation of the associated coordinate s is uniquely defined.

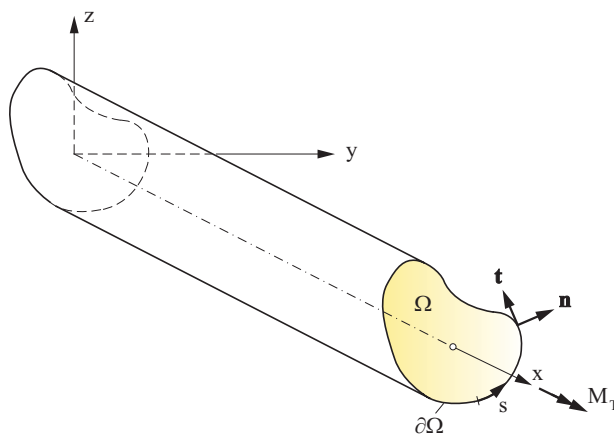


Figure 1: Torsion of a prismatic bar

Twisting of the bar by a torque M_T yields a rotation $\chi = \theta x$, where $\chi \ll 1$. Thus, $\chi = 0$ is assumed at $x = 0$. Within the Saint–Venant torsion theory the usual kinematic assumption for the displacement field reads

$$u_x = \theta w \quad u_y = -\theta xz \quad u_z = \theta xy \quad (1)$$

where, $w(y, z)$ denotes the warping function. With constant twist θ the longitudinal displacement u_x does not depend on x . One can easily show, that only for circular cross-sections $w \equiv 0$ holds, e.g. [2].

The shear strains are obtained by partial derivatives, denoted by commas, as

$$\boldsymbol{\gamma} = \begin{bmatrix} \gamma_{xy} \\ \gamma_{xz} \end{bmatrix} = \begin{bmatrix} u_{x,y} + u_{y,x} \\ u_{x,z} + u_{z,x} \end{bmatrix} = \theta \begin{bmatrix} w_{,y} - z \\ w_{,z} + y \end{bmatrix}. \quad (2)$$

The other strains $\varepsilon_x, \varepsilon_y, \varepsilon_z, \gamma_{yz}$ are identically zero.

Furthermore, it is assumed that the stress components $\sigma_x, \sigma_y, \sigma_z$ and τ_{xy} vanish. Thus, only equilibrium of shear stresses $\boldsymbol{\tau} = [\tau_{xy}, \tau_{xz}]^T$ has to be fulfilled.

The lateral surface of the bar is traction free. Consequently, the vector $\boldsymbol{\tau}$ must be perpendicular to \mathbf{n} on $\partial\Omega$. This is illustrated by the plots of the shear stress vectors in the section on the examples. Hence, neglecting body forces, the boundary value problem reads

$$\tau_{xy,y} + \tau_{xz,z} = 0 \quad \text{in } \Omega \quad \boldsymbol{\tau}^T \mathbf{n} = \tau_{xy} n_y + \tau_{xz} n_z = 0 \quad \text{on } \partial\Omega. \quad (3)$$

One obtains the associated weak form by weighting the differential equations (3)₁ with test functions $\delta w \in \mathcal{V}$ out of $\mathcal{V} = \{\delta w \in H^1(\Omega), \delta w = 0 \text{ on } \partial\Omega_w\}$. Hence, integration over the domain Ω yields

$$g(w, \delta w) = - \int_{(\Omega)} (\tau_{xy,y} + \tau_{xz,z}) \delta w \, dA = 0 \quad (4)$$

and with integration by parts

$$g(w, \delta w) = \int_{(\Omega)} (\tau_{xy} \delta w_{,y} + \tau_{xz} \delta w_{,z}) \, dA - \int_{(\partial\Omega)} (\tau_{xy} n_y + \tau_{xz} n_z) \delta w \, ds = 0. \quad (5)$$

Considering (3)₂ we observe that the boundary integral vanishes.

With the constitutive law of the next section equation (5) becomes nonlinear. For an iterative solution with Newton's method the linearization must be derived. One obtains

$$L[g(w, \delta w)] = g(w, \delta w) + Dg(w, \delta w) \cdot \Delta w = \int_{(\Omega)} \delta \boldsymbol{\gamma}^T \left(\boldsymbol{\tau} + \frac{\partial \boldsymbol{\tau}}{\partial \boldsymbol{\gamma}} \Delta \boldsymbol{\gamma} \right) \, dA \quad (6)$$

where

$$\delta \boldsymbol{\gamma} = \theta \begin{bmatrix} \delta w_{,y} \\ \delta w_{,z} \end{bmatrix} \quad \Delta \boldsymbol{\gamma} = \theta \begin{bmatrix} \Delta w_{,y} \\ \Delta w_{,z} \end{bmatrix} \quad (7)$$

denote the variation and linearization of the strain vector, respectively.

3 Constitutive model

We introduce the standard elastic–plastic rate model according to eq. (8). The shear strains are decomposed in an additive way where the elastic part is described using a linear constitutive relation and the shear modulus G . Furthermore, we assume v.Mises yield condition with linear isotropic hardening and associated flow rule.

$$\begin{aligned}
 \gamma &= \gamma^{el} + \gamma^{pl} \\
 \boldsymbol{\tau} &= G \boldsymbol{\gamma}^{el} \\
 F(\boldsymbol{\tau}, e_v) &= |\boldsymbol{\tau}| - k(e_v) \\
 k(e_v) &= k_0 + \xi e_v \quad k_0 = \frac{y_0}{\sqrt{3}} \\
 \dot{\boldsymbol{\gamma}}^{pl} &= \dot{\lambda} \frac{\partial F}{\partial \boldsymbol{\tau}} = \dot{\lambda} \mathbf{N} \quad \mathbf{N} = \frac{\boldsymbol{\tau}}{|\boldsymbol{\tau}|} \\
 \dot{e}_v &= |\dot{\boldsymbol{\gamma}}^{pl}| = \dot{\lambda} \\
 \dot{\lambda} &\geq 0 \quad F(\boldsymbol{\tau}, e_v) \leq 0 \quad \dot{\lambda} F = 0 \\
 \dot{\lambda} \dot{F} &= 0
 \end{aligned} \tag{8}$$

The yield function according to eq. (8)₃ describes a circle with radius $r = k(e_v)$. The initial radius follows from the yield stress y_0 . The hardening function k depends linearly on the equivalent plastic strains e_v and the plastic tangent modulus ξ . Thus, hardening leads to an enlargement of the radius. The loading and unloading conditions must hold for the flow rule and the evolution law for the equivalent plastic strains.

In case of loading with $\dot{\lambda} > 0$ enforcement of the consistency condition $\dot{\lambda} \dot{F} = 0$ yields the parameter $\dot{\lambda}$

$$\dot{\lambda} = \frac{G}{G + \xi} \mathbf{N} \cdot \dot{\boldsymbol{\gamma}} \tag{9}$$

Hence, it is shown that the equations in (8) are fulfilled with

$$\begin{aligned}
 \boldsymbol{\tau} &= k(e_v) \mathbf{N} \\
 e_v &= \frac{G|\boldsymbol{\gamma}| - k_0}{G + \xi} \\
 \mathbf{N} &= \frac{\boldsymbol{\gamma}}{|\boldsymbol{\gamma}|}
 \end{aligned} \tag{10}$$

First, it is evident that (10) fulfills a priori the yield condition. Considering (8) and (10) one can see that \mathbf{N} is given with

$$\mathbf{N} = \frac{\boldsymbol{\gamma}}{|\boldsymbol{\gamma}|} = \frac{\boldsymbol{\gamma}^{el}}{|\boldsymbol{\gamma}^{el}|} = \frac{\boldsymbol{\gamma}^{pl}}{|\boldsymbol{\gamma}^{pl}|}. \tag{11}$$

Next we introduce the orthogonal vector \mathbf{T} by

$$\mathbf{T} \cdot \mathbf{N} = 0 \quad |\mathbf{T}| = 1 \tag{12}$$

and form the scalar product $\mathbf{T} \cdot \dot{\boldsymbol{\gamma}}$ with $\dot{\boldsymbol{\gamma}} = \dot{\boldsymbol{\gamma}}^{el} + \dot{\boldsymbol{\gamma}}^{pl}$

$$\mathbf{T} \cdot \dot{\boldsymbol{\gamma}} = \mathbf{T} \cdot \left(\frac{1}{G} \dot{\boldsymbol{\tau}} + \dot{\lambda} \mathbf{N} \right) = \frac{1}{G} \mathbf{T} \cdot (\dot{k} \mathbf{N} + k \dot{\mathbf{N}}) = \frac{k}{G} \mathbf{T} \cdot \dot{\mathbf{N}}. \quad (13)$$

Inserting

$$\begin{aligned} \dot{\mathbf{N}} &= \frac{1}{|\boldsymbol{\gamma}^{el}|} [\dot{\boldsymbol{\gamma}}^{el} - (\mathbf{N} \cdot \dot{\boldsymbol{\gamma}}^{el}) \mathbf{N}] \\ \mathbf{T} \cdot \dot{\boldsymbol{\gamma}} &= \mathbf{T} \cdot \dot{\boldsymbol{\gamma}}^{el} \end{aligned} \quad (14)$$

into (13) leads to

$$\left(1 - \frac{k}{G |\boldsymbol{\gamma}^{el}|} \right) \mathbf{T} \cdot \dot{\boldsymbol{\gamma}}^{el} = 0 \quad (15)$$

With $k = |\boldsymbol{\tau}| = G |\boldsymbol{\gamma}^{el}|$ we observe that (15) is identically fulfilled.

In the same way we form the scalar product $\mathbf{N} \cdot \dot{\boldsymbol{\gamma}}$ which yields

$$\mathbf{N} \cdot \dot{\boldsymbol{\gamma}} = \mathbf{N} \cdot \left(\frac{1}{G} \dot{\boldsymbol{\tau}} + \dot{\lambda} \mathbf{N} \right) = \frac{1}{G} \mathbf{N} \cdot (\dot{k} \mathbf{N} + k \dot{\mathbf{N}}) + \dot{\lambda} \quad (16)$$

Considering

$$\dot{\mathbf{N}} \cdot \mathbf{N} = 0 \quad \dot{k} = \dot{\lambda} \xi \quad (17)$$

one obtains

$$\mathbf{N} \cdot \dot{\boldsymbol{\gamma}} = \dot{\lambda} \left(1 + \frac{\xi}{G} \right) \quad (18)$$

which leads to eq. (9).

The equivalent plastic strain is given considering (11)

$$\begin{aligned} e_v &= |\boldsymbol{\gamma}^{pl}| = |\boldsymbol{\gamma} - \boldsymbol{\gamma}^{el}| \\ &= (|\boldsymbol{\gamma}| - \frac{k}{G}) |\mathbf{N}| = |\boldsymbol{\gamma}| - \frac{k_0 + e_v \xi}{G}. \end{aligned} \quad (19)$$

Thus, rewriting (19) gives e_v according to (10)₂. The time derivative yields with (9) and (10)₃

$$\dot{e}_v = \frac{G}{G + \xi} \frac{\boldsymbol{\gamma}}{|\boldsymbol{\gamma}|} \cdot \dot{\boldsymbol{\gamma}} = \dot{\lambda}. \quad (20)$$

The plastic strains $\boldsymbol{\gamma}^{pl} = e_v \mathbf{N}$ and the equivalent plastic strains e_v have to be stored in a history array.

Finally, we summarize the stress computation as

$$\boldsymbol{\tau} = \begin{cases} G (\boldsymbol{\gamma} - \boldsymbol{\gamma}^{pl}) & \text{if } F(\boldsymbol{\tau}^{tr}, e_v^{tr}) \leq 0 \\ k \mathbf{N} & \text{if } F(\boldsymbol{\tau}^{tr}, e_v^{tr}) > 0 \end{cases} \quad (21)$$

where $F(\boldsymbol{\tau}^{tr}, e_v^{tr}) = G |\boldsymbol{\gamma}| - (k_0 + \xi e_v^{tr})$. Here, k follows with (8)₄ and (10)₂, whereas e_v^{tr} and $\boldsymbol{\gamma}^{pl}$ represent the stored plastic strains.

For the linearized boundary value problem (6) the linearization of the stress vector has to be specified. One obtains

$$\mathbf{C}_T := \frac{\partial \boldsymbol{\tau}}{\partial \boldsymbol{\gamma}} = \begin{cases} G \mathbf{1} & \text{if } F(\boldsymbol{\tau}^{tr}, e_v^{tr}) \leq 0 \\ G (\beta \mathbf{1} - \bar{\beta} \mathbf{N} \mathbf{N}^T) & \text{if } F(\boldsymbol{\tau}^{tr}, e_v^{tr}) > 0 \end{cases} \quad (22)$$

with $\beta = \frac{k}{G |\boldsymbol{\gamma}|}$ and $\bar{\beta} = \beta - \frac{\xi}{G + \xi}$.

4 Finite element formulation

The linearized weak form is solved approximately using the finite element method. Within an isoparametric concept the coordinates $\mathbf{x} = [y, z]^T$, the test functions δw and the increments of the warping function Δw are interpolated by

$$\mathbf{x}^h = \sum_{I=1}^{nel} N_I \mathbf{x}_I, \quad \theta \delta w^h = \sum_{I=1}^{nel} N_I \delta w_I, \quad \theta \Delta w^h = \sum_{K=1}^{nel} N_K \Delta w_K. \quad (23)$$

Here, $N_I = N_I(\xi, \eta)$ and $nel = 4, 9, 16, \dots$ denote the shape functions defined on a unit square and the number of nodes per element, respectively.

The variation and linearization of the strains considering (7) yields

$$\begin{aligned} \delta \boldsymbol{\gamma}^h &= \sum_{I=1}^{nel} \mathbf{B}_I \delta w_I & \Delta \boldsymbol{\gamma}^h &= \sum_{K=1}^{nel} \mathbf{B}_K \Delta w_K \\ \mathbf{B}_I &= \begin{bmatrix} N_{I,y} \\ N_{I,z} \end{bmatrix} & \mathbf{B}_K &= \begin{bmatrix} N_{K,y} \\ N_{K,z} \end{bmatrix}. \end{aligned} \quad (24)$$

Inserting eq. (24) into the linearized weak form (6) leads to

$$L[g(w^h, \delta w^h)] = \bigcup_{e=1}^{numel} \sum_{I=1}^{nel} \sum_{K=1}^{nel} \delta w_I (f_I^e + K_{IK}^e \Delta w_K) = 0. \quad (25)$$

The operator \bigcup describes the assembly and $numel$ the total number of finite elements to solve the problem. The stiffness part K_{IK}^e to the nodes I and K as well as the right hand side f_I^e yields

$$f_I^e = \int_{(\Omega_e)} \mathbf{B}_I^T \boldsymbol{\tau} \, dA \quad K_{IK}^e = \int_{(\Omega_e)} \mathbf{B}_I^T \mathbf{C}_T \mathbf{B}_K \, dA \quad (26)$$

with the finite element approximation of $\boldsymbol{\tau}$ and \mathbf{C}_T according to eq. (21) and (22).

Equation (25) leads to a linear system of equations with unknown quantities Δw_K . The boundary condition $\Delta w_I = 0$ must be considered to solve the system, where I is an arbitrary node. The nodal values of the warping function w_I are obtained adding the increments within Newton's method.

Having the warping function $\theta w^h = \sum_{I=1}^{nel} N_I w_I$ we are able to determine the final stress state. Hence, the torsion moment

$$M_T = \int_{(\Omega)} (\tau_{xz}y - \tau_{xy}z) \, dA \quad (27)$$

can now be calculated as a function of the twist θ . In particular, M_T^{el} is that moment where with increasing twist one or various points of the cross-section start to plastify. Here, singular points are excluded within the stress distribution. The associated twist follows from $\theta^{el} = M_T^{el}/(GI_T)$. Furthermore, M_T^{pl} denotes the ultimate torque where the cross-section is completely plastified. Thus, we are able to compute $\kappa = M_T^{pl}/M_T^{el} \geq 1$ as a section quantity.

On symmetry axes the warping function is zero. This can be considered within the discretization. A discussion on the so-called unit warping function which fulfills certain orthogonality conditions is given for elasticity in [6]. These transformations are also possible for elastic-plastic material behaviour.

5 Examples

The developed finite element formulation has been implemented in an enhanced version of the program FEAP, documented in a basic version in [7]. For some simple geometries like rectangular, triangular and circular cross-sections analytical solutions are available, e.g. [2]. These are verified by the numerical solutions. Furthermore we investigate the load carrying behaviour of an H-beam and a bridge transition profile subjected to torsion. The material data are chosen for all examples as

$$G = 81000 \text{ kN/cm}^2 \quad y_0 = 24 \text{ kN/cm}^2 \quad \xi = 0. \quad (28)$$

We use the theoretical value of M_T^{el} as reference quantity in the tables and torque-twist diagrams. For the last two examples where theoretical solutions are not available we take the result for M_T^{pl} of the finest mesh. The final state of the numerical computation is designated as fully plastic state.

5.1 Rectangular cross-section

A rectangle with edge lengths $a = 5 \text{ cm}$ and $b = 10 \text{ cm}$ is considered first. The analytical solutions for M_T^{el} , M_T^{pl} and I_T read

$$\begin{aligned} M_T^{el} &= 0.246 k_0 b a^2 &= 852.2 \text{ kNcm} \\ M_T^{pl} &= \frac{1}{6} k_0 a^2 (3b - a) &= 1443.4 \text{ kNcm} \\ I_T &= 0.229 b a^3 &= 286.25 \text{ cm}^4. \end{aligned} \quad (29)$$

We discretize one quarter using four-node elements. The results of the computation for three different meshes are given in table 1.

Table 1: Ultimate torque and shape factor for different meshes

mesh	M_T^{pl} in kNcm	κ
2×4	1454.7	1.707
10×20	1443.4	1.694
20×40	1443.4	1.694
analytical	1443.4	1.694

Fig. 2 shows the torque-twist diagram with related quantities. The curves approach the theoretical shape factor $\kappa = 1.694$. The approach is quite rapid: $M_T/M_T^{pl} = 0.99$ when $\theta/\theta^{el} = 6$. As can be seen the coarse mesh leads to sufficient accurate results. In Fig. 3 the distribution of the absolute value of the shear stress vectors is given. The plot shows that almost the complete cross-section retains the shear yield stress k_0 and therefore is practically completely plastified. The shear stress vectors and the warping function are plotted in Fig. 4 and Fig. 5 for the elastic and ultimate state, respectively. For this example the sand-heap analogy yields a body with the form of a pyramid. The slope of

the surface corresponds to the shear yield stress k_0 , see Fig. 3. Finally using the finest mesh we start unloading at $\theta/\theta^{el} = 10$ until the resulting torque vanishes, see Fig. 2. The associated residual stress state is depicted in Fig. 6. The maximum absolute value of the shear stresses $|\boldsymbol{\tau}| = 12.45 \text{ kN/cm}^2$ is considerable.

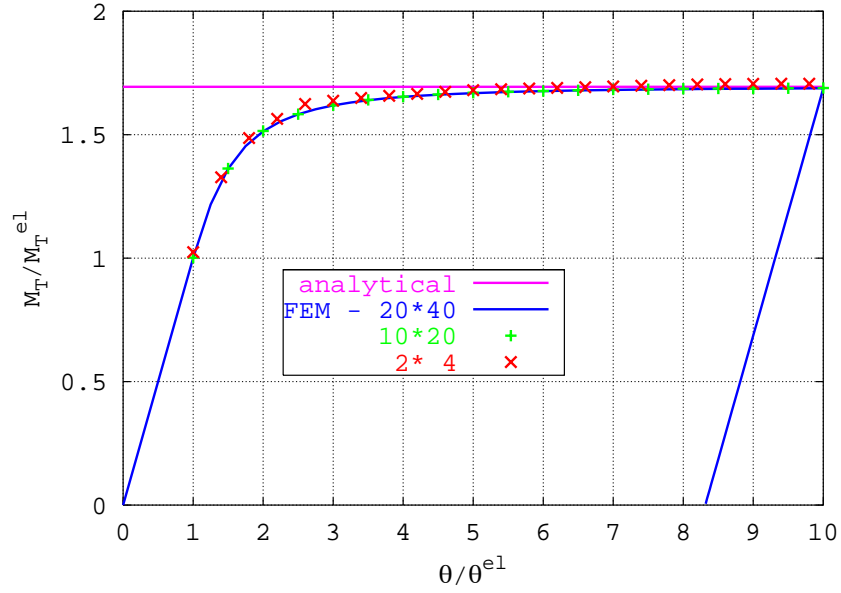


Figure 2: Torque–twist diagram for the rectangle

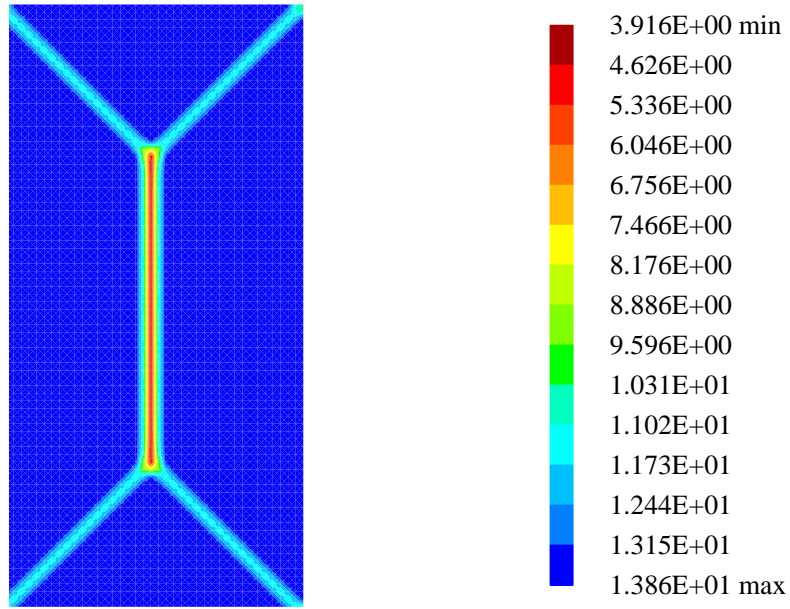


Figure 3: Absolute value of shear stress vector in the fully plastic state

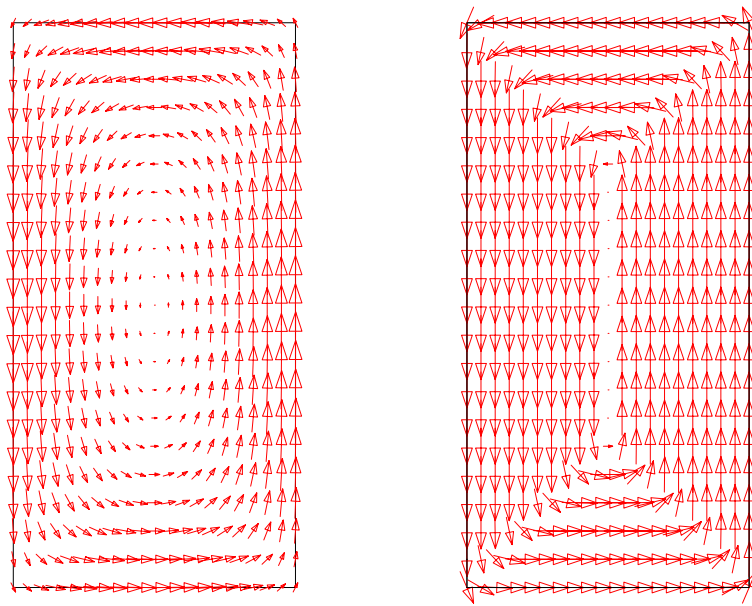


Figure 4: Shear stress vectors in the elastic and fully plastic state

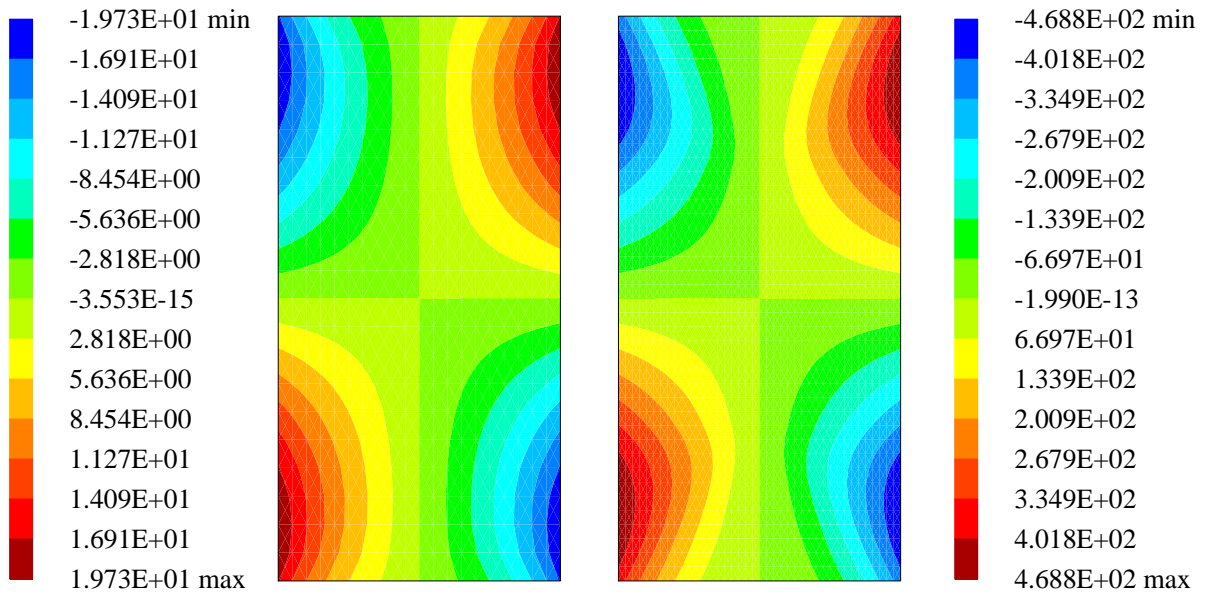


Figure 5: Warping function in the elastic and fully plastic state

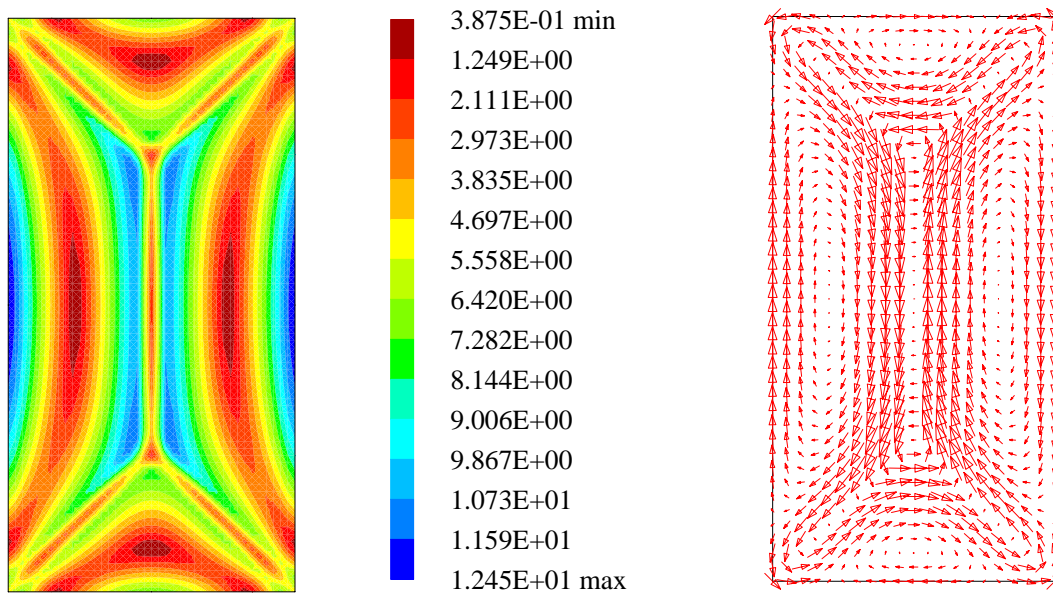


Figure 6: Residual stresses of the unloaded state, absolute values and directions of shear stress vectors

5.2 Triangular cross-section

As second example we investigate an equilateral triangle with edge lengths $a = 10 \text{ cm}$. The following analytic values for M_T^{el} , M_T^{pl} and I_T are given

$$\begin{aligned} M_T^{el} &= k_0 h^3/13 = 692.3 \text{ kNcm} \\ M_T^{pl} &= k_0 a^3/12 = 1154.7 \text{ kNcm} \\ I_T &= h^4/26 = 216.35 \text{ cm}^4 \end{aligned} \tag{30}$$

where $h = 0.5\sqrt{3}a$.

A discretization considering symmetries and using four-node elements is shown in Fig. 7. The ultimate torques and shape factors are given in table 1 for three different meshes. In Fig. 8 the torque-twist diagram is depicted. The theoretical shape factor $\kappa = 1.668$ is approached asymptotically as $\theta \rightarrow \infty$. In Fig. 9 the absolute values of the shear stress vectors are plotted. One can see in a top view the ridge line of a triangular pyramid. Thereby the sand heap analogy is visualized for this example. In Fig. 10 and 11 the directions of the shear stress vectors and the warping function are shown for the elastic and ultimate state, respectively.

Table 2: Ultimate torque and shape factor for different meshes.

FE-mesh	M_T^{pl} in $kNcm$	κ
96 elements	1156.8	1.671
261 elements	1154.7	1.668
582 elements	1154.7	1.668
analytical	1154.7	1.668

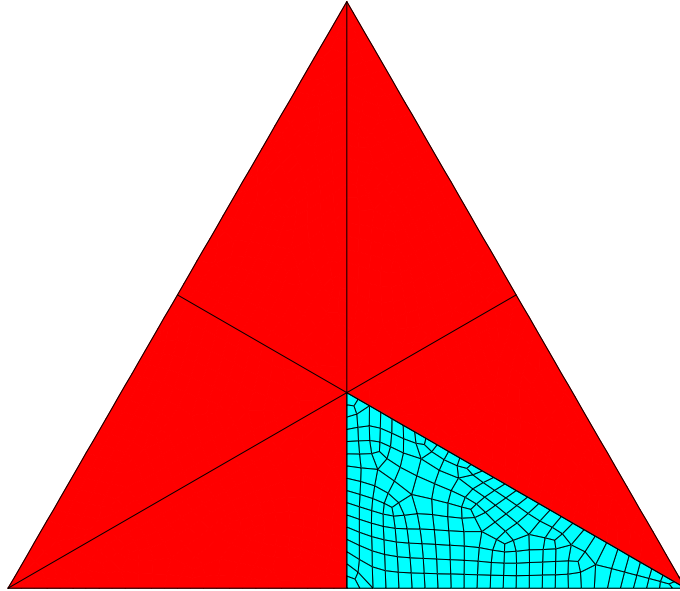


Figure 7: Discretization of one sixth of a triangular cross-section

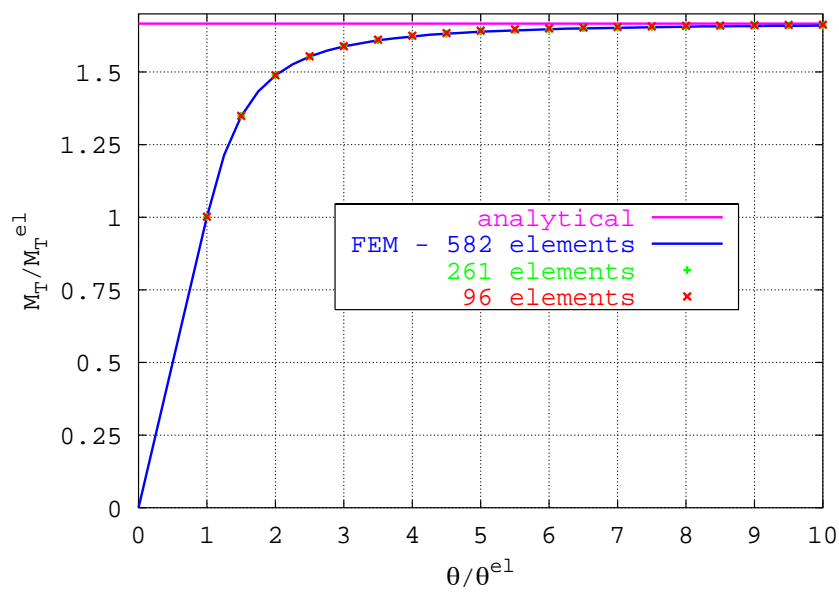


Figure 8: Torque-twist diagram of the triangle

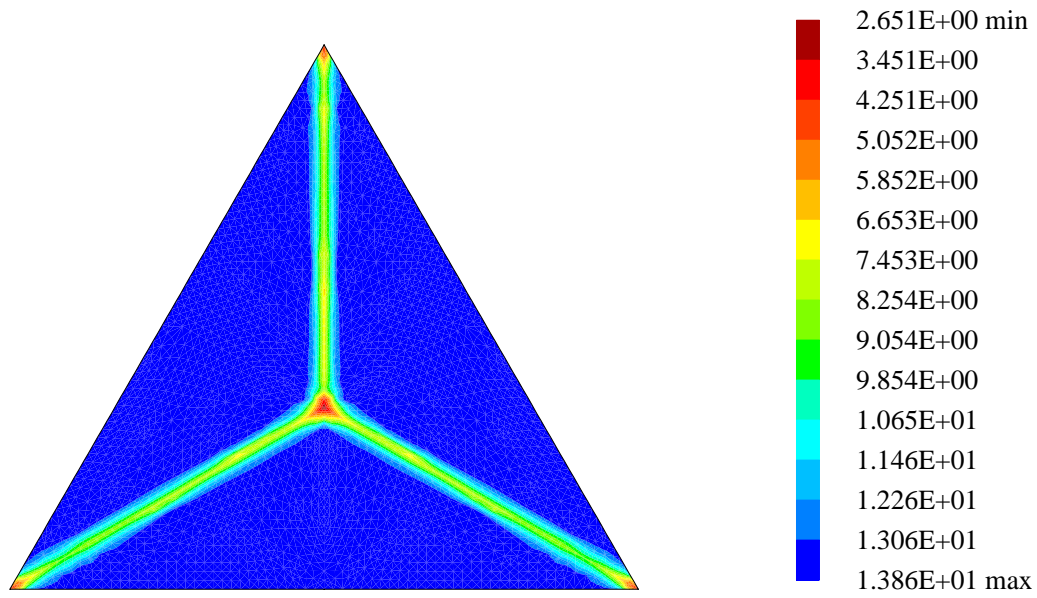


Figure 9: Absolute value of shear stress vector in the fully plastic state

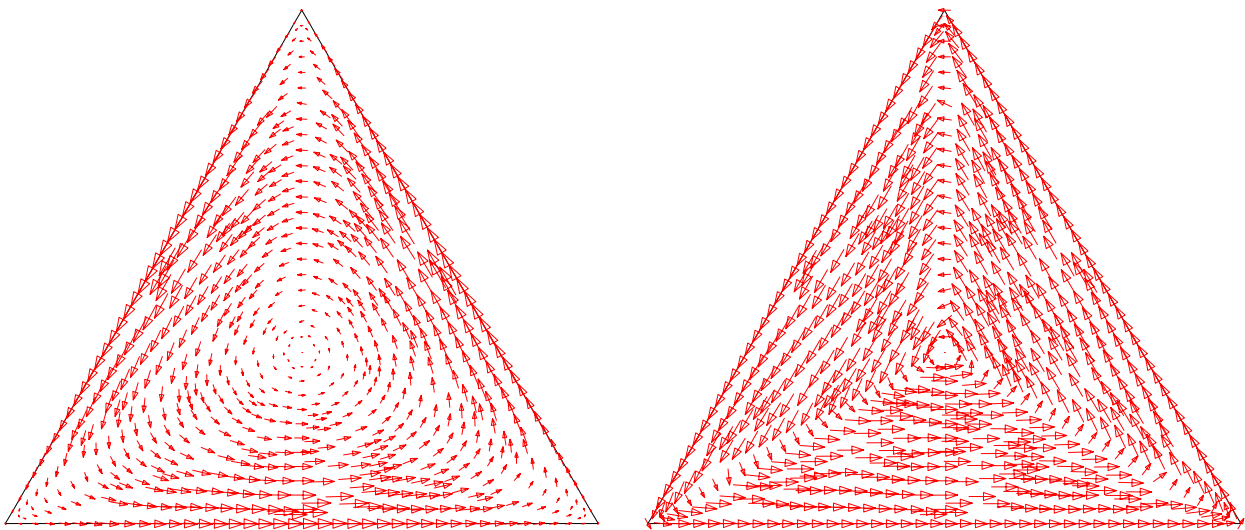


Figure 10: Shear stress vectors in the elastic and fully plastic state

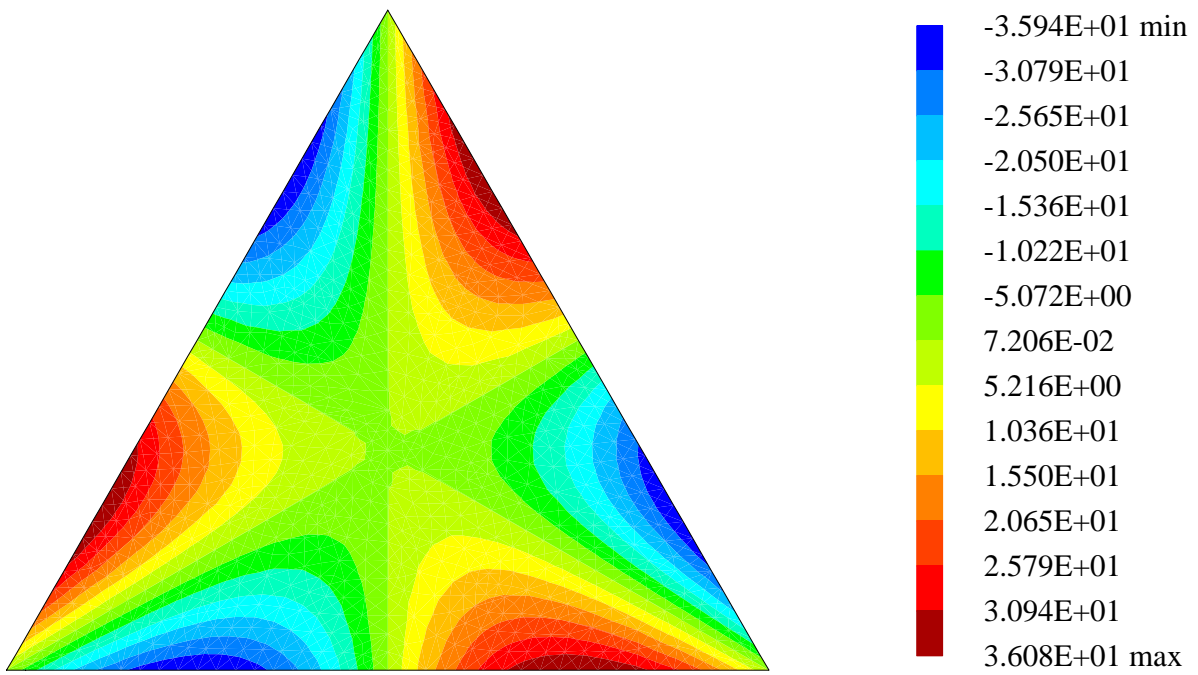
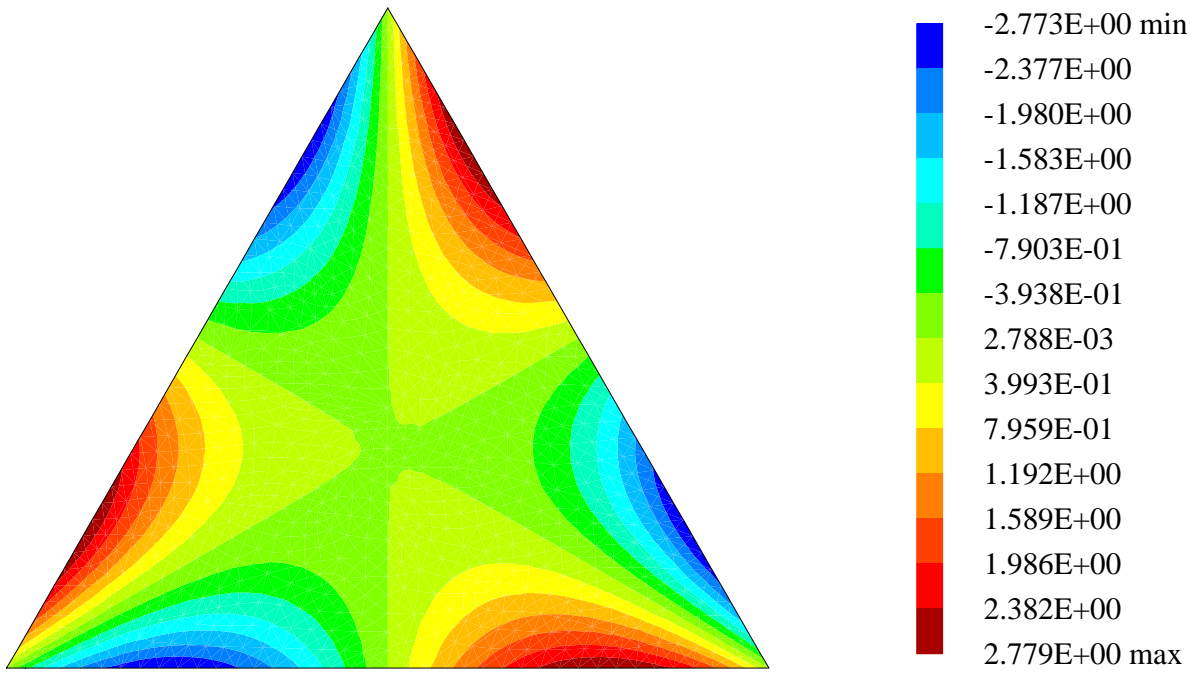


Figure 11: Warping function in the elastic and fully plastic state

5.3 Hollow circular shaft

The developed finite element formulation is also valid for multiple connected domains. As example we consider an annular space with outer and inner radius $a = 10\text{ cm}$ und $b = 5\text{ cm}$. The analytic solution for this example reads

$$M_T = 2\pi k_0 \left(\frac{a^3}{3} - \frac{b^4}{4r} - \frac{r^3}{12} \right) \quad a \geq r = \frac{k_0}{G\theta} \geq b. \quad (31)$$

Hence, evaluation at $r = a$ and $r = b$ yields

$$\begin{aligned} M_T^{el} &= \frac{1}{2a} \pi k_0 (a^4 - b^4) = 20405.2 \text{ kNcm} \\ M_T^{pl} &= \frac{2}{3} \pi k_0 (a^3 - b^3) = 25393.2 \text{ kNcm} \end{aligned} \quad (32)$$

and from that the shape factor $\kappa = 1.244$. The elastic–plastic solution is valid for $\theta^{el} \leq \theta \leq \theta^{pl}$, where $\theta^{el} = k_0/Ga$. In this case the approach is not asymptotic. The ultimate torque is attained at $\theta^{pl} = k_0/Gb = 2\theta^{el}$.

A finite element discretization of a quarter is shown in Fig. 12. To obtain stable equilibrium iterations even in the fully plastic state we assume a small plastic tangent modulus $\xi = 10^{-5}G$. The results of the numerical computation with the finest mesh according to diagram 13 show very good agreement with the analytic solution. For this example with $w \equiv 0$, each point of the solution curve can be attained in a single load step without any equilibrium iterations. Fig. 14 shows the absolute value of the shear stress vectors. Finally, in Fig. 15 the resultant shear stresses are depicted for the elastic and fully plastic case.

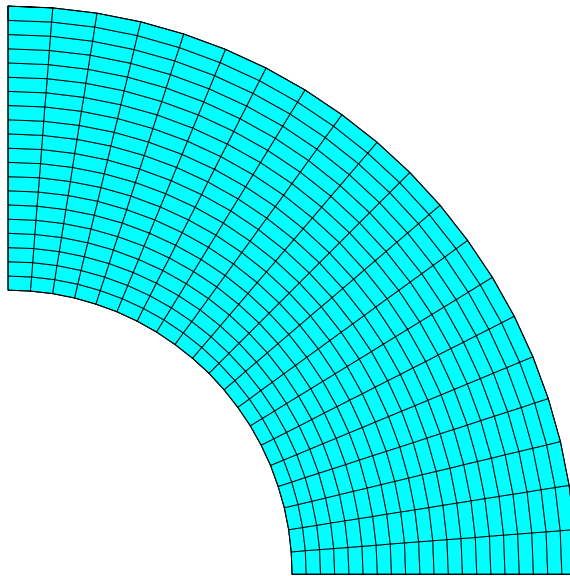


Figure 12: Discretization of the hollow circular shaft

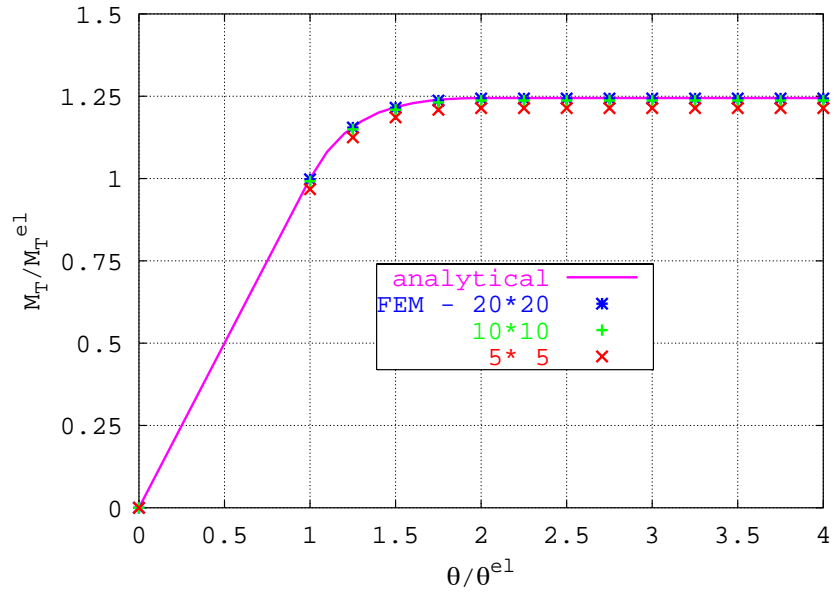


Figure 13: Torque–twist diagram of the hollow circular shaft

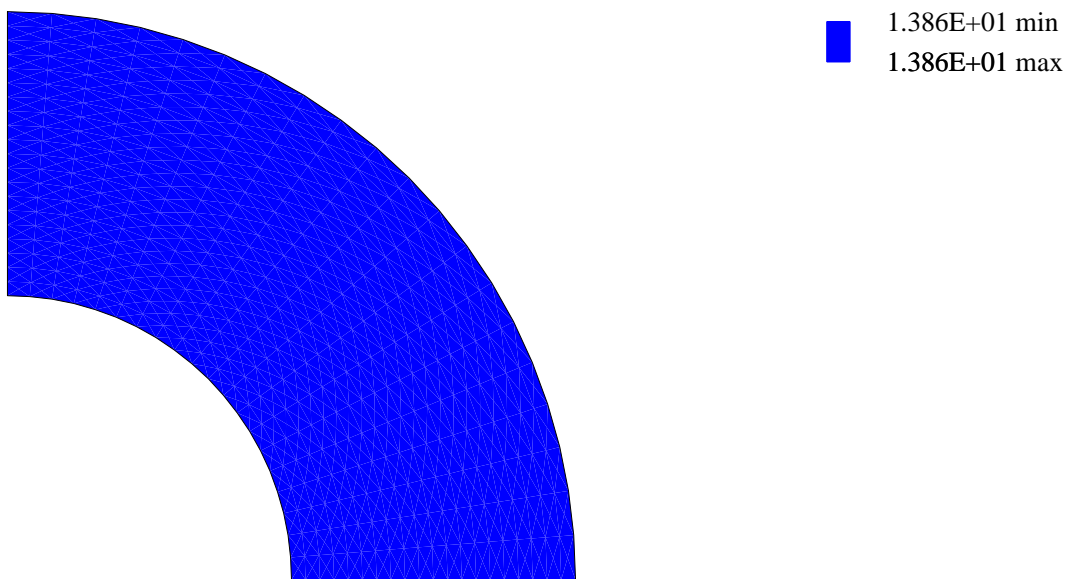


Figure 14: Absolute value of shear stress vectors in the fully plastic state

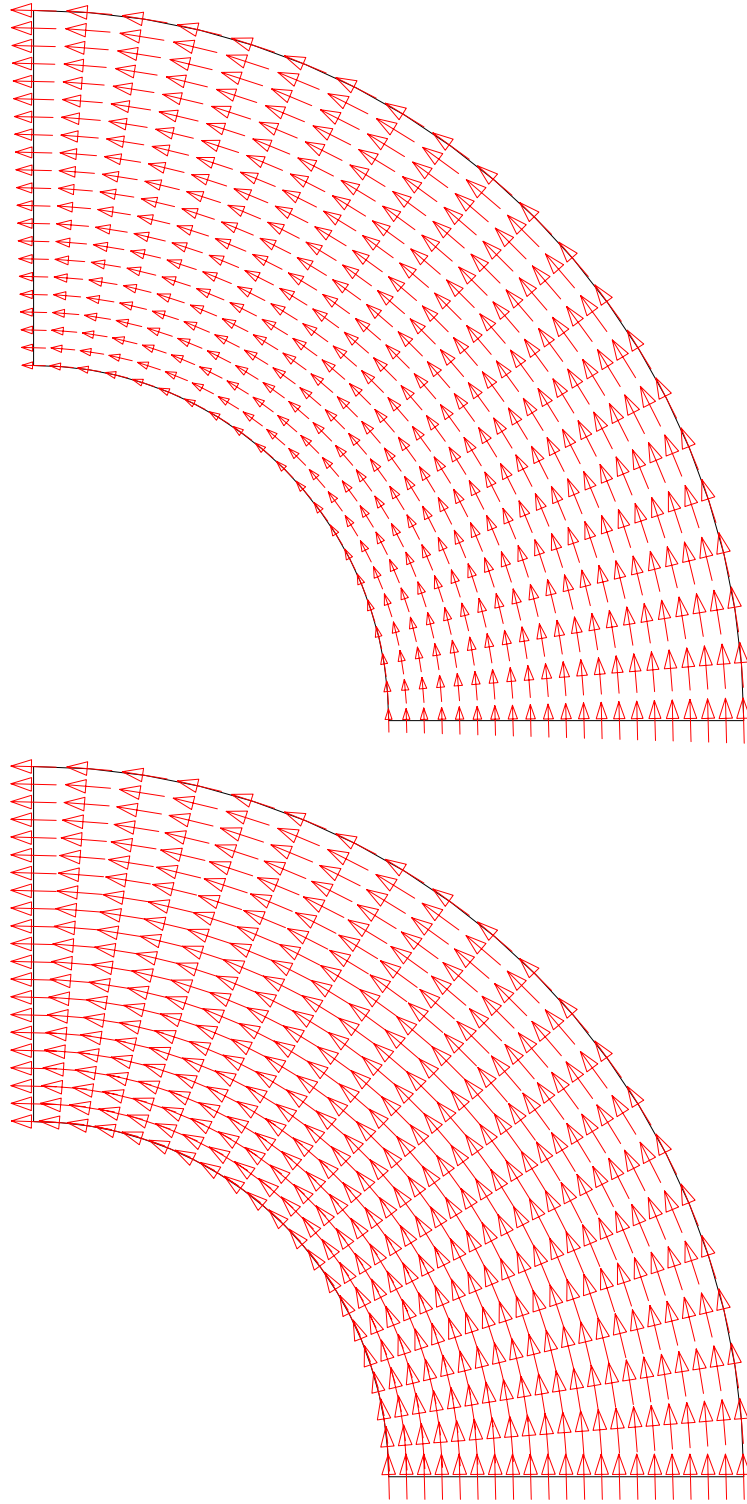


Figure 15: Shear stress vectors in the elastic and fully plastic state

5.4 Rolled–steel section HEM–300

Next we investigate a rolled–steel section according to DIN 1025 Teil 4 (10.63). A discretization of a quarter is depicted in Fig. 16. With the finest mesh we obtain $M_T^{el} = 3583.1 \text{ kNcm}$. The Saint–Venant torsion modulus reads $I_T = 1414.9 \text{ cm}^4$.

In table 3 the computed values for M_T^{pl} und κ are given. Thus, the shape factor $\kappa = 2.119$ is considerable. The torque–twist curves are depicted for different meshes in diagram 17. As can be seen the coarse mesh yields sufficient accurate results. Fig. 18 yields the distribution of the absolute value of the shear stress vector. The plot shows in a top view the ridge lines applying the sand–heap analogy. Finally, in Fig. 19 the shear stress vectors are plotted for the elastic and fully plastic state.

Table 3: Section quantities for a HEM 300

FE–mesh	M_T^{pl} in kNcm	κ
534 elements	7599.4	2.121
1235 elements	7599.4	2.121
4190 elements	7592.6	2.119

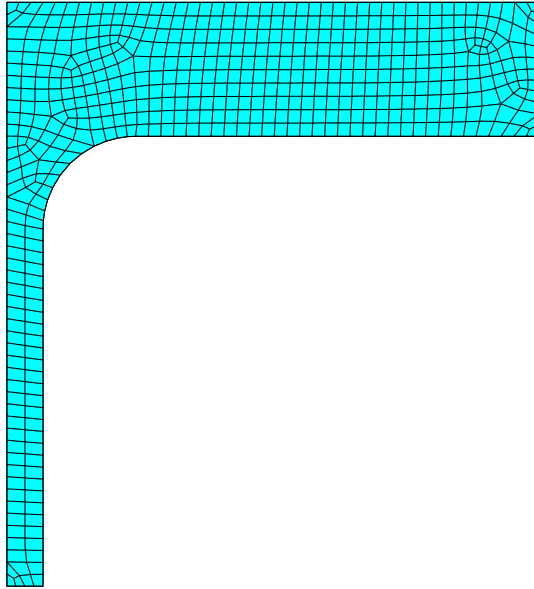


Figure 16: Discretization of a quarter HEM–300 using 534 elements

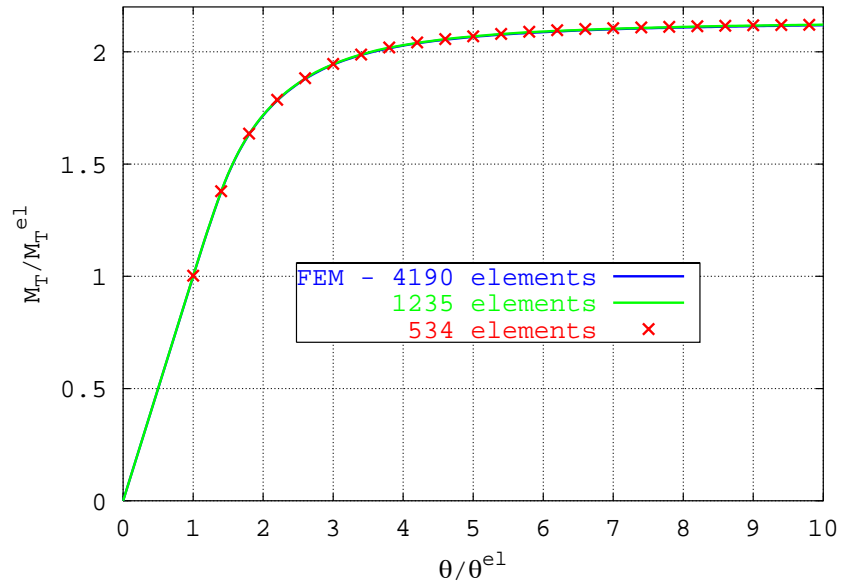


Figure 17: Torque–twist diagram of a HEM–300

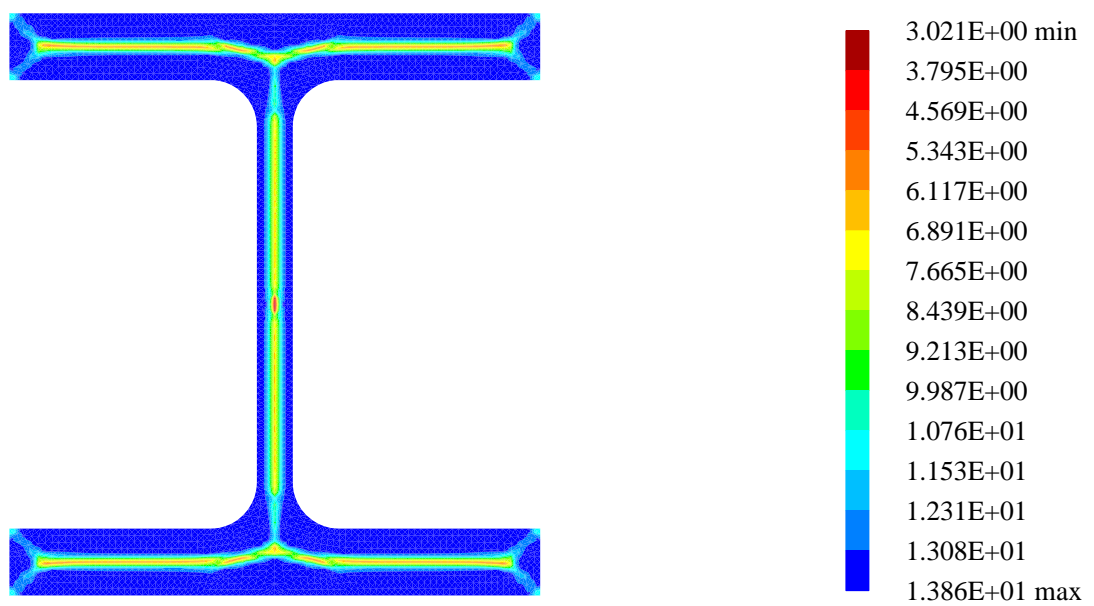


Figure 18: Absolute value of the shear stress vectors in the fully plastic state

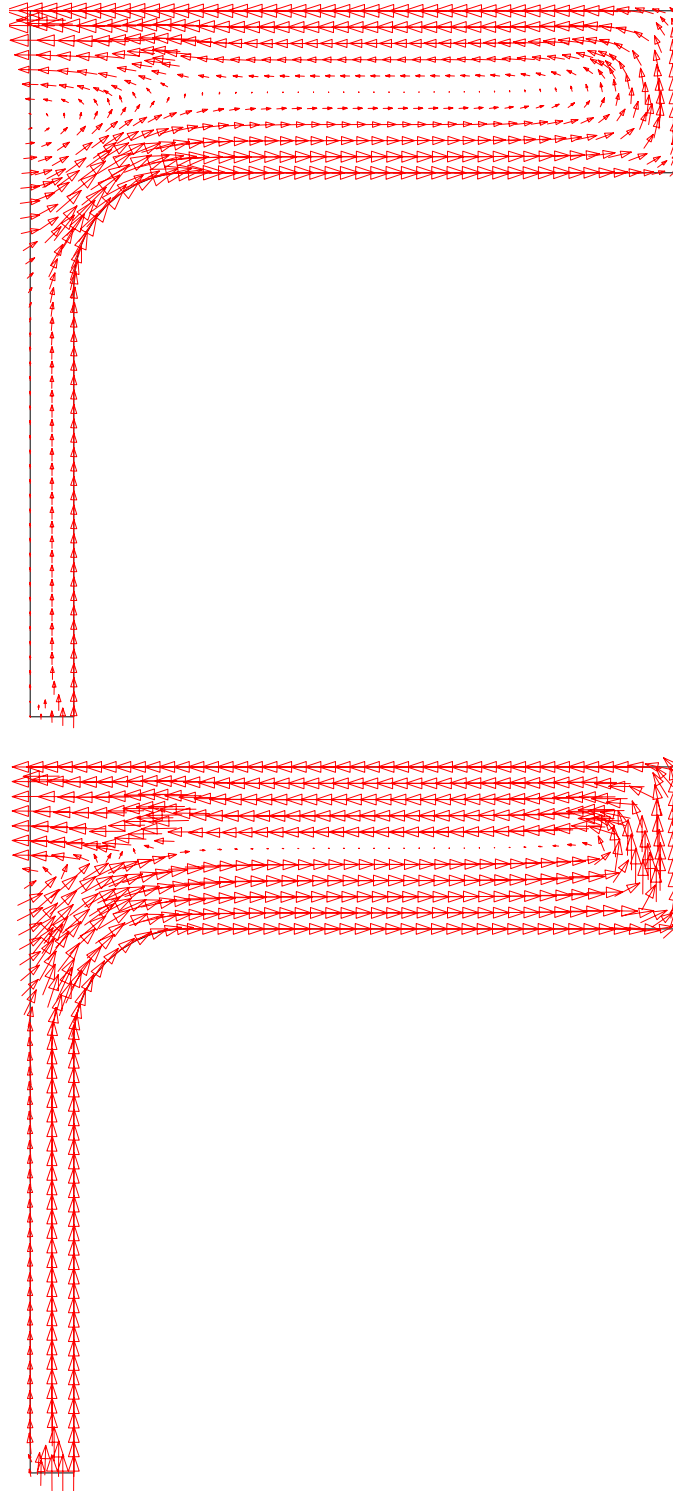


Figure 19: Shear stress vectors in the elastic and fully plastic state

5.5 Bridge transition profile

As last example we consider the rather complicated cross-section according to Fig. 20. Such profiles are used in bridge transition constructions. Considering symmetry half of the domain is discretized using different meshes. The section quantities M_T^{pl} and κ are computed and summarized in Table 4. Furthermore the twist $\theta^{el} = M_T^{el}/(G I_T)$ follows with $M_T^{el} = 2828.0 \text{ kNcm}$ and $I_T = 2223.7 \text{ cm}^4$. The resulting shape factor $\kappa = 2.728$ describes a considerable section reserve. The torque-twist curves according to Fig. 21 depict the results using the coarse meshes. Finally the absolute value and the directions of the shear stress vectors are plotted in Fig. 22 and 23, respectively.

Table 4: Section quantities of a bridge transition profile

FE-mesh	M_T^{pl} in $kNcm$	κ
478 elements	7765.8	2.746
817 elements	7754.5	2.742
1860 elements	7731.9	2.734
3378 elements	7720.6	2.730
5376 elements	7714.9	2.728

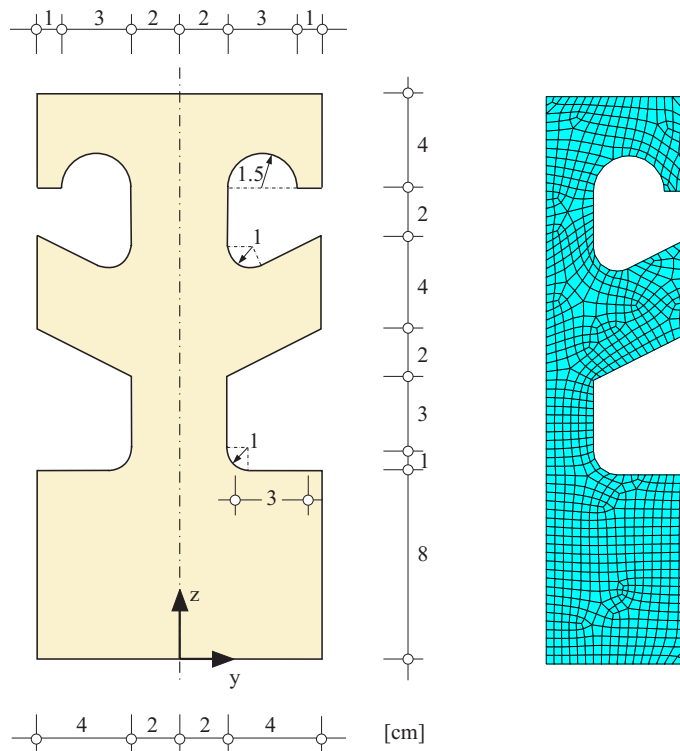


Figure 20: Geometry and discretization of a bridge transition profile

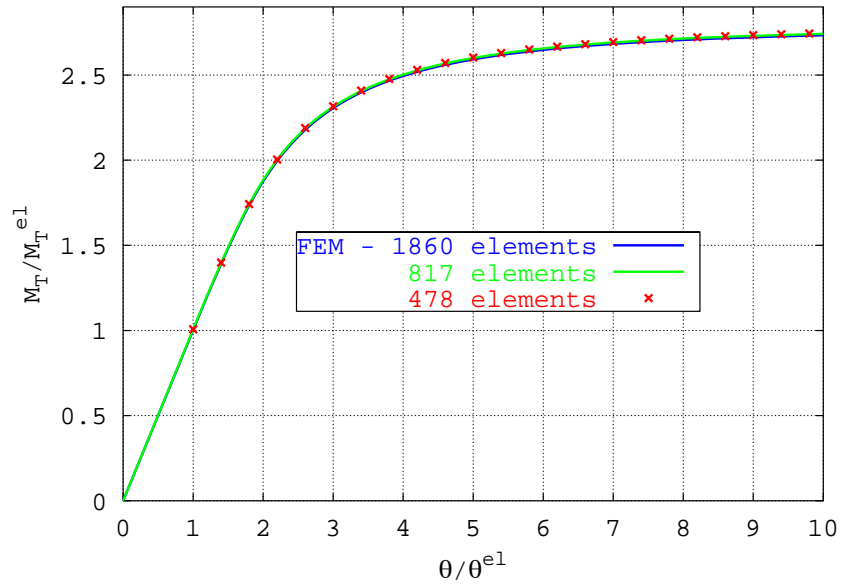


Figure 21: Torque–twist diagram of a bridge transition profile

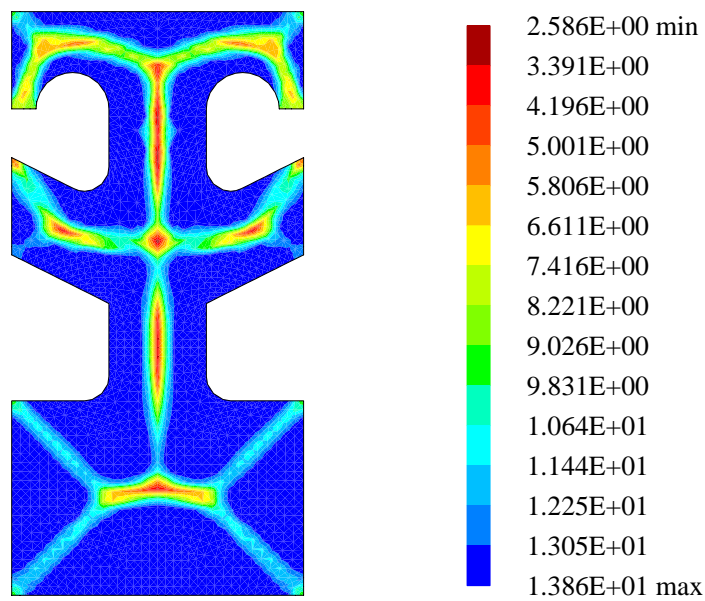


Figure 22: Absolute value of shear stress vector in the fully plastic state

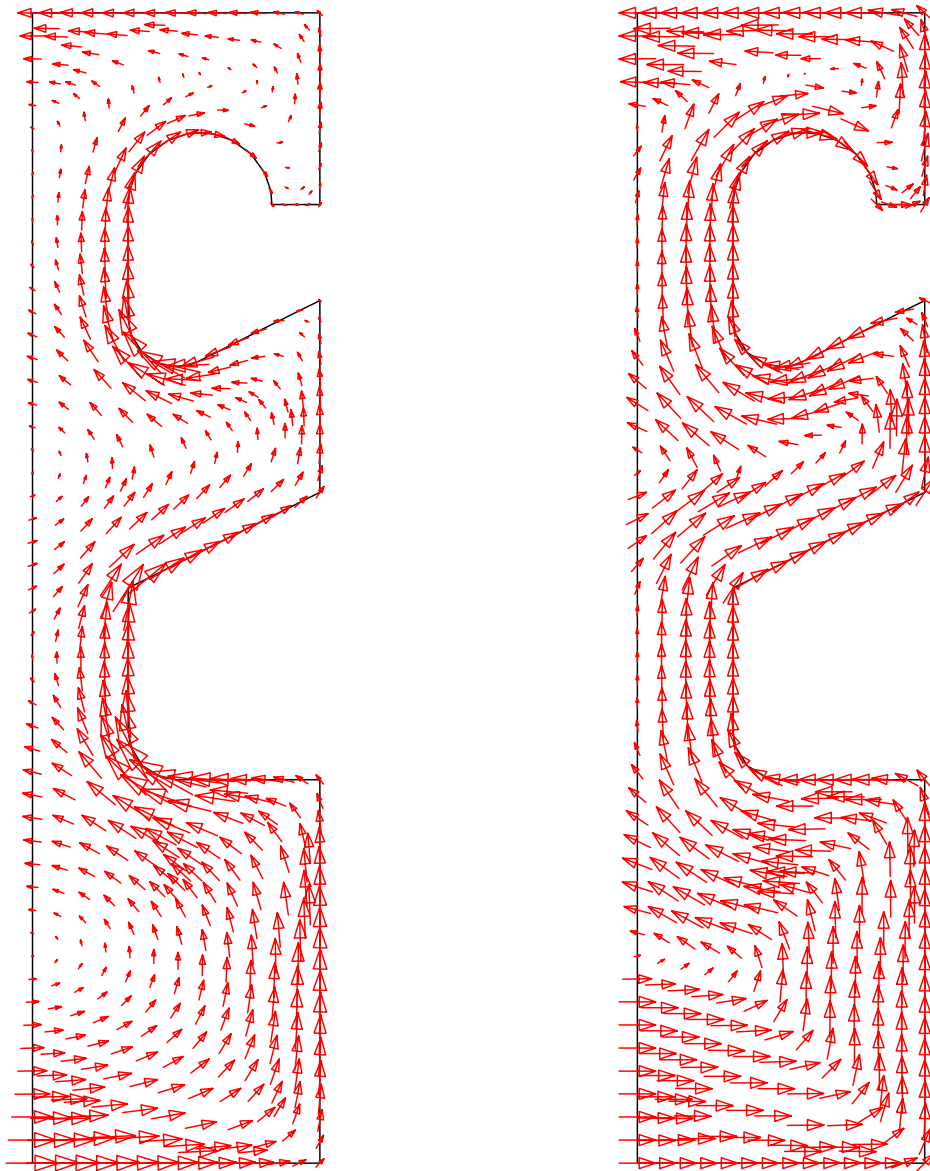


Figure 23: Shear stress vectors in the elastic and fully plastic state

6 Conclusions

Based on the equations of the Saint–Venant torsion theory and assuming an elastic–plastic material law the variational equations and an associated finite element formulation are derived. Applying line search techniques within the equilibrium iterations the fully plastic torsion moment can be calculated in one load step. The computed results are in very good agreement with available analytic solutions for simple geometric shapes. Application of the sand–heap analogy shows plausibility of the computed stress field. Thus, the developed finite element formulation is a robust tool to compute the ultimate torque for arbitrary shaped cross–sections of prismatic bars.

References

- [1] I. S. Sokolnikoff, *Mathematical Theory of Elasticity*, (McGraw–Hill, New York, 1956).
- [2] J. Lubliner, *Plasticity Theory*, (Macmillan Publishing Company New York, Collier Macmillan Publishers, London 1990).
- [3] A. Nádai, Der Beginn des Fließvorganges in einem tordierten Stab, *ZAMM* 3 (1923) 442–454.
- [4] Y. Yamada, S. Nakagiri and K. Takatsuka, Elastic–Plastic Analysis of Saint–Venant Torsion Problem by a hybrid Stress Model, *Int. J. Num. Meth. Engng.* 5 (1972) 193–207.
- [5] S. Baba and T. Kajita, Plastic Analysis of Torsion of a Prismatic Beam, *Int. J. Num. Meth. Engng.* 18 (1982) 927–944.
- [6] F. Gruttmann, R. Sauer and W. Wagner, Shear stresses in prismatic beams with arbitrary cross–sections, *Int. J. Num. Meth. Engng.* 45 (1999) 865–889.
- [7] O.C. Zienkiewicz and R.L. Taylor, *The Finite Element Method*, Vol. 2, 4th edition, (McGraw–Hill, London, 1989).